# $\alpha$ effect in a turbulent liquid-metal plane Couette flow

G. Rüdiger*
*Leibniz Institute for Astrophysics Potsdam, An der Sternwarte 16, D-14482 Potsdam, Germany*
*and Helmholtz-Zentrum Dresden-Rossendorf, P.O. Box 510119, D-01314 Dresden, Germany*

A. Brandenburg
*Nordita, KTH Royal Institute of Technology and Stockholm University, Roslagstullsbacken 23, SE-10691 Stockholm, Sweden*
*and Department of Astronomy, Stockholm University, SE-10691 Stockholm, Sweden*

(Received 8 December 2013; published 11 March 2014)

We calculate the mean electromotive force in plane Couette flows of a nonrotating conducting fluid under the influence of a large-scale magnetic field for driven turbulence. A vertical stratification of the turbulence intensity results in an $\alpha$ effect owing to the presence of horizontal shear. Here we discuss the possibility of an experimental determination of the components of the $\alpha$ tensor using both quasilinear theory and nonlinear numerical simulations. For magnetic Prandtl numbers of the order of unity, we find that in the high-conductivity limit the $\alpha$ effect in the direction of the flow clearly exceeds the component in spanwise direction. In this limit, $\alpha$ runs linearly with the magnetic Reynolds number Rm, while in the low-conductivity limit it runs with the product $\mathrm{Rm}\cdot\mathrm{Re}$, where Re is the kinetic Reynolds number, so that for a given Rm the $\alpha$ effect grows with decreasing magnetic Prandtl number. For the small magnetic Prandtl numbers of liquid metals, a common value for the horizontal elements of the $\alpha$ tensor appears, which makes it unimportant whether the $\alpha$ effect is measured in the spanwise or the streamwise directions. The resulting effect should lead to an observable voltage of about 0.5 mV in both directions for magnetic fields of 1 kG and velocity fluctuations of about 1 m/s in a channel of 50-cm height (independent of its width).

DOI: 10.1103/PhysRevE.89.033009 PACS number(s): 47.27.ek

## I. INTRODUCTION

Mean-field electrodynamics of turbulent conducting fluids provides the commonly accepted approach to explaining the existence of magnetic fields of cosmic bodies. The excitation of magnetic fields results from the interplay of two elementary processes, diffusive and nondiffusive ones. It is known that turbulent motions reduce large-scale electric currents by inducing an electromotive force (EMF) opposite to the direction of the current. One can write

$$\overline{\boldsymbol{u}\times\boldsymbol{b}} = -\mu_0\eta_T\overline{\boldsymbol{J}}, \tag{1}$$

where $\boldsymbol{\mathcal{E}} = \overline{\boldsymbol{u}\times\boldsymbol{b}}$ is the EMF, with $\boldsymbol{u} = \boldsymbol{U} - \overline{\boldsymbol{U}}$ and $\boldsymbol{b} = \boldsymbol{B} - \overline{\boldsymbol{B}}$ being the fluctuating contributions to the velocity $\boldsymbol{U}$ and magnetic field $\boldsymbol{B}$, respectively, overbars denote averaging (to be specified later), $\mu_0$ is the vacuum permeability, $\boldsymbol{J} = \mathrm{rot}\boldsymbol{B}/\mu_0$ is the current density, and $\eta_T$ is the turbulent magnetic diffusivity. In stellar convection zones, $\eta_T$ exceeds the molecular (microphysical) value $\eta$ of the magnetic diffusivity by many orders of magnitude.

In this paper the EMF is derived for a turbulent fluid in the presence of a mean shear flow $\overline{\boldsymbol{U}}$ and a *uniform* background field $\overline{\boldsymbol{B}}$. For a turbulent dynamo, the enhanced dissipation must be overcome by an induction process that does not run with the electric current. One also knows that under the influence of global rotation and a uniform magnetic field, anisotropic turbulence produces an EMF parallel to the field [1]; i.e.,

$$\overline{\boldsymbol{u}\times\boldsymbol{b}} = \alpha\overline{\boldsymbol{B}} - \cdots. \tag{2}$$

Here, $\alpha$ is a pseudoscalar formed by the rotation vector $\boldsymbol{\Omega}$ and the anisotropy direction $\boldsymbol{g}$ with $\alpha \propto \boldsymbol{g}\cdot\boldsymbol{\Omega}$. Often, the anisotropy direction from the gradient of density stratification of the fluid is used, but it is also possible that an intensity gradient close to rigid boundaries forms the preferred direction. The resulting dynamo equation in rotating and stratified plasma is [1]

$$\frac{\partial\bar{\boldsymbol{B}}}{\partial t} = \mathrm{rot}(\alpha\bar{\boldsymbol{B}} - (\eta+\eta_T)\mathrm{rot}\bar{\boldsymbol{B}}), \tag{3}$$

which has nondecaying solutions if $\alpha$ exceeds a critical value ("$\alpha^2$ dynamo"); see Ref. [2] for a review.

In many papers the presented concept of a turbulent dynamo has been applied to planets, stars, accretion disks, galaxies, and galaxy clusters; see references in [3]. Very few papers, however, deal with an experimental confirmation of the validity of relations (1) and (2) in the laboratory. This is surprising given the astrophysical importance of Eq. (3) as a direct consequence of Eqs. (1) and (2), which characterizes the basic ingredients of electrodynamics in rotating turbulent fluid conductors. Generally, the validity of Eq. (1) is not seriously doubted. However, the existing laboratory experiments report an increase in the effective magnetic diffusivity by only a few percent [4]. This is because the molecular magnetic diffusivity is rather large and the turbulence not strong enough. This is an unfortunate situation, as the eddy concept of the effective dissipation in turbulent media governs much of cosmic physics, from climate research, to geophysics, to the theory of star formation and quasars.

An even more dramatic situation holds with respect to the $\alpha$ effect. There are one or two experiments on the basis of the idea that the $\alpha$ effect is essentially a measure of the swirl of the flow. It has been demonstrated that a fluid with imposed

*gruediger@aip.de

 

helicity (imposed by rigid, swirling channels) produces an EMF in the direction of an imposed field; see Refs. [5–7]. It has not yet been shown, however, that a rotating fluid with helicity that is *not* imposed (but results from the global rotation of the fluid) leads to an observable $\alpha$ effect. In natural cosmic bodies, helicity is usually due to the interaction of rotating turbulence with density stratification. The aim of the present paper is to suggest a more rigorous $\alpha$ effect experiment. As we demonstrate, the difficulties in such an experiment make it understandable that this has not yet been possible without the use of a prescribed helicity.

It is easy to see the general difficulty of performing $\alpha$ effect experiments. Using Eq. (2), the potential difference between the endplates of the container in the direction of the mean magnetic field is

$$\Delta\Phi = \alpha \overline{B} H, \tag{4}$$

where $H$ is the distance between the endplates. Hence, for $H \simeq 100$ cm and $B \simeq 1000$ G (say), the potential difference is $\Delta\Phi = 1$ mV for $|\alpha| = 1$ cm/s. The maximum $\alpha$ value is of the order of $u_{\rm rms}$, hence $\Delta\Phi \lesssim u_{\rm rms}$ (in mV). For $u_{\rm rms} \simeq 1$ cm/s the maximally induced potential difference is therefore 1 mV. A container of 5-cm radius rotating at 1 Hz has a linear outer velocity of more than 30 cm/s so that $u_{\rm rms} \simeq 1$ cm/s might be considered a conservative estimate. We find that, as a necessary condition for any $\alpha$ experiment, one must be able to measure potential differences *smaller* than a few millivolts. The $\alpha$ experiment in Riga [5] worked with $B \simeq 1$ kG and velocities of the order of meters per second, so that the $\Delta\Phi$ exceeded 10 mV. This experiment, however, used a prescribed helical geometry to mimic the symmetry breaking between left- and right-handed helicities.

If the rotation is not uniform, the resulting shear induces toroidal magnetic fields so that for sufficiently strong shear the $\alpha$ effect can be rather small and still produce a dynamo ("$\alpha\Omega$ dynamo"). It is well known that also turbulence in liquid metals subject to a plane shear flow (without rotation!) is able to work as a dynamo if the turbulence intensity is stratified in the direction orthogonal to the shear flow plane; see Ref. [8]. The basic rotation may thus not be the only flow whose influence enables the turbulence to generate global magnetic fields.

In the present paper, a plane Couette flow is considered to analyze the characteristic issues of the corresponding $\alpha$ effect and to design a possible experiment to measure its amplitude.

## II. THE MEAN ELECTROMOTIVE FORCE

Consider a plane shear flow with uniform vorticity in the vertical $z$ direction, i.e.,

$$\bar{U}_y = Sx, \tag{5}$$

where $S$ is the shear rate. The shear flow may exist in a turbulence field that does not possess anisotropy other than that induced by the shear, (5), itself. The one-point correlation tensor is

$$Q_{ij} = \overline{u_i(\boldsymbol{x},t) u_j(\boldsymbol{x},t)}. \tag{6}$$

The correlation tensor may be constructed by a perturbation method. The fluctuating velocity field is represented by a series expansion,

$$\boldsymbol{u} = \boldsymbol{u}^{(0)} + \boldsymbol{u}^{(1)} + \boldsymbol{u}^{(2)} + \cdots, \tag{7}$$

where the superscript index shows the order of the contributions in terms of the mean shear flow.

The zero-order term represents the "original" isotropic turbulence, which is assumed to be not yet influenced by the shear. We denote the Fourier transform of the correlation tensor with a hat and define the spectral tensor for the original turbulence as

$$\hat{Q}^{(0)}_{ij} = \frac{E(k,\omega)}{16\pi k^2}\left(\delta_{ij} - \frac{k_i k_j}{k^2}\right), \tag{8}$$

where the positive-definite spectrum $E$ gives the intensity of isotropic fluctuations with

$$\overline{\boldsymbol{u}^{(0)2}} = \int_0^\infty \int_0^\infty E(k,\omega) dk d\omega. \tag{9}$$

Here, $\boldsymbol{k}$ and $\omega$ are the wave vector and frequency. For analytical calculations, the one-parametric spectrum,

$$E(k,\omega) = \frac{2}{\pi}\frac{w}{\omega^2 + w^2}\hat{E}(k), \tag{10}$$

can be used, which yields a $\delta$ function, $E \propto \delta(\omega)$, in the limit of $w \to 0$ and leads to a white-noise spectrum for large $w$. The correlation time of the turbulence is defined as $\tau_{\rm corr} = 1/w$. The extremely short correlation times of white noise automatically lead to the high-conductivity limit for all fluid conductors with a finite magnetic diffusivity $\eta$. On the other hand, the application of (10) in the form of a $\delta$ function provides the result in the low-conductivity limit.

By definition, the magnetic diffusivity tensor relates the mean EMF, (1), to gradients of the mean magnetic field via the relation $\mathcal{E}_i = \eta_{ijk}\bar{B}_{j,k}$. This tensor for originally isotropic turbulence, influenced by the mean shear flow, (5), has been constructed up to first order in the shear [8,10]. In that work, it was also shown that the combination of shear and the shear-induced parts of the magnetic diffusion tensor is not able to operate as a dynamo.

On the other hand, it has been shown in Ref. [8] that shear, in combination with *stratified* turbulence, provides helicity that leads to an $\alpha$ effect in Eq. (2). Here, $\alpha$ must be a pseudotensor so that an $\epsilon$ tensor has to appear in the coefficients for $\alpha$. The construction of the EMF, $\mathcal{E}_i = \epsilon_{ijk}\overline{u_j b_k}$, is the only possibility for the $\epsilon$ tensor to appear. The subscript of $\mathcal{E}_i$ is therefore always also a subscript of the $\epsilon$ tensor. As the $\epsilon$ tensor is of rank 3, an inhomogeneity of turbulence with the stratification vector $\boldsymbol{g} = \nabla \log u^2_{\rm rms}$ and $u_{\rm rms} = \sqrt{\overline{u^2}}$ must also be present for the $\alpha$ effect to exist. If shear is included to first order, the general structure of the $\alpha$ tensor is

$$\begin{aligned}\alpha_{ij} = {} & \gamma\epsilon_{ijk}g_k + (\alpha_1\epsilon_{ikl}\bar{U}_{j,k} + \alpha_2\epsilon_{ikl}\bar{U}_{k,j})g_l \\ & + \alpha_3\epsilon_{ikl}g_j\bar{U}_{l,k} + \alpha_4\epsilon_{ikj}\bar{U}_{l,k}g_l + \alpha_5\epsilon_{ijk}\bar{U}_{k,l}g_l.\end{aligned} \tag{11}$$

If the stratification is along the vertical $z$ axis, it follows from (11) that, for the horizontal components of the $\alpha$ tensor,

$$\begin{aligned}\alpha_{xx} &= \alpha_2 g_z S = \alpha_x S, \\ \alpha_{yy} &= -\alpha_1 g_z S = \alpha_y S, \\ \alpha_{xy} &= -\alpha_{yx} = \gamma g_z = \Gamma.\end{aligned} \tag{12}$$

Turbulent pumping is characterized by $\alpha_{xy}$. The anisotropy of the $\alpha$ tensor is described by the difference between $\alpha_x$ and $\alpha_y$. In the adopted geometry, the azimuthal component $\alpha_{yy}$ (the coefficient $\alpha_1$ defined below) plays the main role in all cosmic applications, while in the proposed experiment with a turbulent shear flow the coefficient $\alpha_2$ is probed, and it produces the EMF *perpendicular* to the flow.

The coefficients in (12) read

$$\gamma = \frac{1}{6}\int_0^\infty \int_0^\infty \frac{\eta k^2 E(k,\omega)}{\omega^2+\eta^2 k^4} dk\, d\omega \tag{13}$$

for the pumping term and

$$\alpha_n = \int_0^\infty \int_0^\infty A_n E\,(k,\omega)\, dk\, d\omega \tag{14}$$

for the $\alpha$ effect, with

$$\begin{aligned} A_1 &= \frac{4\nu\eta^3 k^8 + 2\omega^2\eta(\nu+\eta)k^4}{15(\omega^2+\nu^2k^4)(\omega^2+\eta^2k^4)^2} + \frac{\eta^2k^4(\eta^2k^4-3\omega^2)}{15(\omega^2+\eta^2k^4)^3}, \\ A_2 &= -\frac{\eta^2\nu^3(4\eta-5\nu)k^{12}}{60(\omega^2+\nu^2k^4)^2(\omega^2+\eta^2k^4)^2} \\ &\quad - \frac{\omega^2\nu(28\eta^3-4\eta^2\nu+12\eta\nu^2+5\nu^3)k^8}{60(\omega^2+\nu^2k^4)^2(\omega^2+\eta^2k^4)^2} \\ &\quad - \frac{\omega^4\eta(\eta+36\nu)k^4-5\omega^6}{60(\omega^2+\nu^2k^4)^2(\omega^2+\eta^2k^4)^2} \end{aligned} \tag{15}$$

for the kernels. Here, $\nu$ is the kinematic viscosity. In the following we define the magnetic Prandtl number as $\mathrm{Pm} = \nu/\eta$. Only the terms occurring in (12) have been given. For small Pm, one can easily estimate the coefficient $\alpha_1$. For $\nu \ll \eta$, the expression for $A_1$ simplifies to

$$A_1 = \frac{1}{15}\frac{1}{(\omega^2+\eta^2k^4)^2}\left\{\frac{4\nu\eta^3k^8}{\omega^2+\nu^2k^4} + \frac{\eta^2k^4(3\eta^2k^4-\omega^2)}{\omega^2+\eta^2k^4}\right\}. \tag{16}$$

For $\nu \to 0$, the first expression on the right-hand side forms a $\delta$ function. Hence,

$$\alpha_1 = \frac{2\pi}{15}\int_0^\infty \frac{E(k,0)}{\eta k^2} dk + \cdots \simeq \frac{2\pi}{15}\mathrm{Rm}\,\ell_{\mathrm{corr}}^2 + \cdots, \tag{17}$$

with the magnetic Reynolds number of the turbulence

$$\mathrm{Rm} = \frac{u_{\mathrm{rms}}^2 \tau_{\mathrm{corr}}}{\eta}. \tag{18}$$

The missing terms in (17), however, are of the same order as the given one, so that it can only be used for orientation. In (17) we have used the estimate

$$\int_0^\infty \frac{E(k,0)}{k^2} dk = \tau_{\mathrm{corr}} u_{\mathrm{rms}}^2 \ell_{\mathrm{corr}}^2, \tag{19}$$

which follows from (10).

As mentioned above, the white-noise approximation mimics the high-conductivity limit, which holds for cosmic applications. In this approach, the spectrum does not depend on the frequency $\omega$ up to a maximum value $\omega_{\max}$, above which the power spectrum vanishes. This corresponds to a turbulence model with a very short correlation time; i.e., $\tau_{\mathrm{corr}} \simeq 1/\omega_{\max}$.

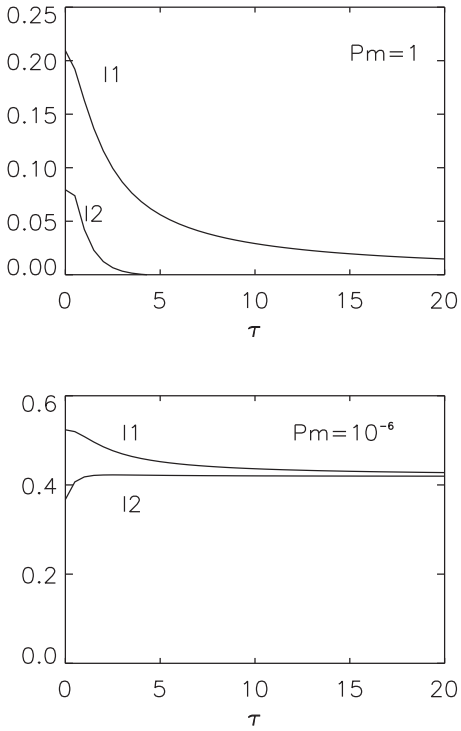


FIG. 1. Numerical values of the coefficients $I_1$ and $I_2$. Top, Pm = 1; bottom, $\mathrm{Pm} = 10^{-6}$ (liquid gallium). Note that in the high-conductivity limit ($\tau \to 0$; white-noise spectrum) the coefficients $I_1$ and $I_2$ for $\mathrm{Pm} \ll 1$ exceed the values for Pm = 1. For small Pm the differences between $I_1$ and $I_2$ and the influence of the diffusivity parameter $\tau$ almost vanish.

One finds from (16), after integration,

$$\alpha_1 = \frac{\pi}{6\eta}\int_0^\infty \frac{E(k,0)}{k^2} dk, \tag{20}$$

so that

$$\alpha_1 = \frac{\pi}{6}\mathrm{Rm}\,\ell_{\mathrm{corr}}^2, \tag{21}$$

which is similar to result (17). The factor $\pi/6$ also appears in Fig. 1 for small Pm as the value of $I_1$ at the left vertical axis for $\tau_{\mathrm{corr}} = 0$. The same procedure for Pm = 1, applied to (15) for $A_1$, leads to

$$\alpha_1 = \frac{\pi}{15}\mathrm{Rm}\,\ell_{\mathrm{corr}}^2. \tag{22}$$

Now, one finds the factor $\pi/15$ on the left vertical axis in Fig. 1 (top) for Pm = 1. Note that the result for small Pm exceeds that for Pm = 1. For given $\eta$, lower values of the viscosity $\nu$ lead to *higher values* of the EMF. It is this unexpected behavior that makes experiments with fluid metals, with their small magnetic Prandtl numbers, very promising.

While very small values of $\tau_{\mathrm{corr}}$ (relative to the magnetic diffusion time $\tau_{\mathrm{diff}}$) represent the high-conductivity limit, a much larger value of $\tau_{\mathrm{corr}}$ represents the low-conductivity limit, which can be treated by assuming $w \to 0$ in Eq. (10), which corresponds to using a $\delta$ function in Eqs. (15). It directly follows from (15) for $A_1$ that

$$\alpha_1 = \frac{1}{15}\left(1+\frac{4}{\mathrm{Pm}}\right)\mathrm{Rm}^2\,\ell_{\mathrm{corr}}^2, \tag{23}$$

so that Pm = 1 leads to $\alpha_1 = \frac{1}{3}\mathrm{Rm}^2\ \ell_{\rm corr}^2$. For small magnetic Prandtl numbers one finds $\alpha_1 = \frac{4}{15}\mathrm{Re\ Rm}\ \ell_{\rm corr}^2$, where Re = Rm/Pm is the Reynolds number. Hence, in the low-conductivity limit (small Rm) the $\alpha$ effect runs with Re · Rm, while in the high-conductivity limit (large Rm) the $\alpha$ effect runs with Rm. Very similar expressions also occur if the shear flow is formally replaced with a basic rotation [11].

The general expression for finite correlation times, which is valid between the high- and the low-conductivity limits, might also be written in the form

$$\alpha_1 = I_1(\tau)\ \mathrm{Rm}\ \ell_{\rm corr}^2, \tag{24}$$

where $I_1(\tau)$ is given in Fig. 1 for Pm = 1 (top) and Pm = $10^{-6}$ (bottom). The curves result from numerical integrations using a spectral function of the form $\exp(-\tau^2\omega^2)$ with the dimensionless parameter,

$$\tau = \eta k^2 \tau_{\rm corr} \simeq 1/\mathrm{Rm}, \tag{25}$$

for the aforementioned ratio of the correlation time to the magnetic diffusion time of the eddies. $\tau < 1$ gives the sector of high conductivity and $\tau > 1$ gives the sector of low conductivity. One finds that for the given range of $\tau$ for small Pm, the function $I_1$ is nearly uniform (in contrast to the case for Pm = 1). The consequence is that, also for lower conductivities, the $\alpha$ effect only decreases linearly with Rm rather than quadratically as is the case for Pm = 1. The appearance of the 1/Pm term in Eq. (23) is the formal reason for this surprising and very promising behavior.

As a demonstration, Fig. 2 shows the behavior of the numerical integrals for decreasing Pm and very large values of $\tau$. The integrals run with $(\mathrm{Pm}\ \tau)^{-1}$ so that for Pm $\tau \gg 1$ the relation $\alpha_1 \propto \mathrm{Re\ Rm}$ results. For small Pm, the kinetic Reynolds number is much larger than the magnetic Reynolds number. For a given magnetic diffusivity, smaller values of the viscosity strongly enhance the resulting $\alpha$ effect.

In experiments with liquid metals like sodium and gallium, Rm is of the order of $0, 1, \ldots, 1$, so $\tau \simeq 1 \ldots 10$. In this regime, and for small Pm, the coefficient $I_1$ hardly changes with $\tau$ (see Fig. 1). Its approximate value is 0.4, which is very close to the value $\pi/6$ valid in the high-conductivity limit. The reason is that for small Pm the transition of $I_1$ to the low-conductivity limit only happens at rather high values of $\tau$ (Fig. 2). In this limit one finds a strong influence of the magnetic Prandtl number.

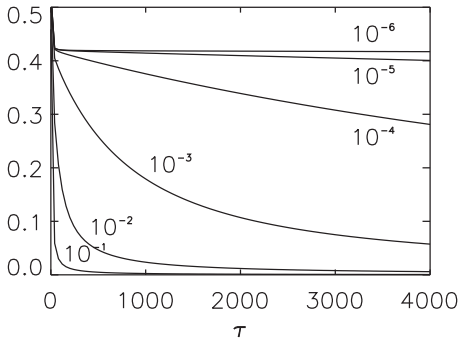


FIG. 2. $I_1$ for various Pm values. Obviously, for a given magnetic diffusivity $\eta$, fluids with a much lower viscosity (like sodium and gallium) are even better qualified for laboratory experiments.

Similar calculations for $\alpha_2$ lead to

$$\alpha_2 \simeq -I_2\ \mathrm{Rm}\ \ell_{\rm corr}^2, \tag{26}$$

where $I_2$ is also plotted in Fig. 1. For $\tau$ of the order of unity and small Pm, we find $I_2 \lesssim I_1 \approx 0.4$, so

$$\alpha_2 \simeq -0.4\ \mathrm{Rm}\ \ell_{\rm corr}^2. \tag{27}$$

In the low-conductivity limit ($\tau \gg 1$), we have

$$\alpha_2 = -\frac{1}{60}\left(\frac{4}{\mathrm{Pm}} - 5\right)\mathrm{Rm}^2\ \ell_{\rm corr}^2, \tag{28}$$

which changes its sign at Pm = 0.8 and yields, for small Pm,

$$\alpha_2 = -\frac{1}{15}\mathrm{Rm\,Re}\ \ell_{\rm corr}^2 = -\alpha_1. \tag{29}$$

Indeed, Fig. 1 shows that for large values of $\tau$ and Pm = 1, $I_2$ is negative (and small), but for Pm $\ll 1$ it is positive ($\simeq$0.4).

In summary, the plots in Fig. 1 reveal an important influence of the value of the viscosity on the $\alpha$ effect for a given diffusivity. For small Pm, using the low-conductivity limit, the ratio of $I_2$ to $I_1$ approaches unity, while for Pm = 1 it is very small. Note that for Pm = 1, $\alpha_1$ strongly exceeds $\alpha_2$, but this is no longer the case for small Pm. The two horizontal components of the $\alpha$ tensor are then of the same order of magnitude. The signs of the components are always identical.

It must also be mentioned that the magnetic Prandtl number is much smaller for liquid metals than what can presently be used in numerical simulations. Figure 1 shows that in numerical simulations, $\alpha_{xx}$ should be smaller than $\alpha_{yy}$; this is not true, however, for laboratory conditions, with their small Pm. In this case it does not matter whether the shear-induced $\alpha$ effect is measured in the streamwise or the spanwise direction.

This finding is in stark contrast to the results of the turbulence model described in [12] for applications to convection zones. This model works with a very steep frequency spectrum, $E \propto \delta(\omega)$, and assumes Pm = $\tau$ = 1 for the diffusivities of a postulated small-scale background turbulence. This immediately leads to $A_2/A_1 = 1/20$; i.e., $\alpha_{xx}/\alpha_{yy} = 1/20$. The considered turbulence model, therefore, yields a strongly dominating $\alpha$ effect in the azimuthal direction (as also in our approach for Pm = 1).

It is also obvious that the pumping term does not depend on the shear. After (13), for small $\eta$, it does not run with $1/\eta$. It is simply

$$\gamma \simeq u_{\rm rms}^2 \tau_{\rm corr} \simeq \eta\ \mathrm{Rm}. \tag{30}$$

It can only be measured if the external field $B_0$ lies in the shear plane.

## III. NUMERICAL SIMULATIONS

It is straightforward to verify the existence of an $\alpha$ effect in a shear flow using numerical simulations of nonuniformly forced turbulent shear flows in Cartesian coordinates. We perform simulations in a cubic domain of size $L^3$, so the minimal wave number is $k \equiv k_1 = 2\pi/L$. We solve the equations of compressible hydrodynamics with an isothermal equation of

state with constant sound speed $c_s$,

$$\frac{\mathrm{D}\boldsymbol{U}}{\mathrm{D}t} = SU_x\hat{\mathbf{y}} - c_s^2\boldsymbol{\nabla}\log\rho + \boldsymbol{f} + \rho^{-1}\boldsymbol{\nabla}\cdot 2\rho\nu\mathsf{S}, \tag{31}$$

$$\frac{\mathrm{D}\log\rho}{\mathrm{D}t} = -\boldsymbol{\nabla}\cdot\boldsymbol{U}, \tag{32}$$

where $\mathrm{D}/\mathrm{D}t = \partial/\partial t + \boldsymbol{U}\cdot\boldsymbol{\nabla} + Sx\,\partial/\partial y$ is the advective derivative with respect to the full velocity field (including the shear flow), $\boldsymbol{U}$ is the departure from the mean shear flow $(0,Sx,0)$, and $\mathsf{S}_{ij} = \frac{1}{2}(\partial_i U_j + \partial_j U_i) - \frac{1}{3}\delta_{ij}\boldsymbol{\nabla}\cdot\boldsymbol{U}$ is the traceless rate of the strain matrix (not to be confused with the shear rate $S$). The flow is driven by a random forcing function $\boldsymbol{f}$ consisting of nonhelical waves with wave numbers whose modulus lie in a narrow band around an average wave number $k_f = 5k_1$ [13]. We arrange the amplitude of the forcing function such that the rms velocity increases with height, while the maximum Mach number remains below 0.1, so the effects of compressibility are negligible. The resulting flow is irregular in space and time and is loosely referred to as turbulence.

We use the kinematic test-field method [9] in the Cartesian implementation [14] to compute from the simulations simultaneously the relevant components of the $\alpha$ effect and turbulent diffusivity tensors, $\alpha_{ij}$ and $\eta_{ij}$. We do this by solving an additional set of equations governing the departure of the magnetic field from a set of given mean fields. This mean field is referred to as a test field and is labeled with a superscript T. For each test field $\overline{\boldsymbol{B}}^{\mathrm{T}}$, we find the corresponding fluctuations $\boldsymbol{b}^{\mathrm{T}} = \mathrm{rot}\boldsymbol{a}^{\mathrm{T}}$ by solving the inhomogeneous equation for the corresponding vector potential $\boldsymbol{a}^{\mathrm{T}}$,

$$\frac{\mathcal{D}\boldsymbol{a}^{\mathrm{T}}}{\mathcal{D}t} = -Sa_y^{\mathrm{T}}\hat{\boldsymbol{x}} + \overline{\boldsymbol{U}}\times\boldsymbol{b}^{\mathrm{T}} + \boldsymbol{u}\times\overline{\boldsymbol{B}}^{\mathrm{T}} + (\boldsymbol{u}\times\boldsymbol{b}^{\mathrm{T}})' + \eta\nabla^2\boldsymbol{a}^{\mathrm{T}}, \tag{33}$$

where $\mathcal{D}/\mathcal{D}t = \partial/\partial t + Sx\,\partial/\partial y$ is the advective derivative with respect to the imposed shear flow only (i.e., without $\boldsymbol{U}$), and $(\boldsymbol{u}\times\boldsymbol{b}^{\mathrm{T}})' = \boldsymbol{u}\times\boldsymbol{b}^{\mathrm{T}} - \overline{\boldsymbol{u}\times\boldsymbol{b}^{\mathrm{T}}}$ is the fluctuating part of $\boldsymbol{u}\times\boldsymbol{b}^{\mathrm{T}}$. We compute the corresponding mean EMF, $\boldsymbol{\mathcal{E}}^{\mathrm{T}} = \overline{\boldsymbol{u}\times\boldsymbol{b}^{\mathrm{T}}}$, which is then related to $\overline{\boldsymbol{b}}^{\mathrm{T}}$ and its curl, $\mu_0\overline{\boldsymbol{J}}^{\mathrm{T}} = \mathrm{rot}\,\overline{\boldsymbol{B}}^{\mathrm{T}}$, via

$$\mathcal{E}_i^{\mathrm{T}} = \alpha_{ij}\overline{B}_j^{\mathrm{T}} - \eta_{ij}\mu_0\overline{J}_j^{\mathrm{T}}. \tag{34}$$

We use four different test fields, with $x$ or $y$ components being proportional to $\sin kz$ or $\cos kz$. The $x$ and $y$ components of Eq. (34) then constitute eight equations for the four relevant components of $\alpha_{ij}(z,t)$ and $\eta_{ij}(z,t)$.

We adopt periodic boundary conditions in the $y$ direction, shearing-periodic boundary conditions in the $x$ direction, and stress-free perfect conductor boundary conditions in the $z$ direction; i.e.,

$$\partial_z u_x = \partial_z u_y = u_z = a_x^{\mathrm{T}} = a_y^{\mathrm{T}} = \partial_z a_z^{\mathrm{T}} = 0. \tag{35}$$

Numerical resolutions of $64^3$ and $128^3$ mesh points were found to be sufficient, depending on the value of Pm. The PENCIL CODE [15] has been used for all calculations.

Simulations are performed for different parameter combinations. The quantities $S$ and $g_z$ are positive in the calculations presented here; i.e., the basic velocity, (5), grows in the positive $x$ direction, while the turbulence intensity grows in the positive $z$ direction. To make contact with laboratory experiments, we focus here on the case of low conductivity and choose $\mathrm{Rm} \equiv u_{\mathrm{rms}}/\eta k_f = 0.2$, which is consistent with our definition of Eq. (18) with a Strouhal number of unity; i.e., $\tau_{\mathrm{corr}}u_{\mathrm{rms}}k_f = 1$. As in earlier work using fully helical turbulence, we present time averages of the components of $\alpha_{ij}$ and $\eta_{ij}$ in normalized form in terms of $\alpha_0 = u_{\mathrm{rms}}/3$ and $\eta_{T0} = u_{\mathrm{rms}}/3k_f$. Hence, $\alpha_0 L/\eta_{T0} = Lk_f = 10\pi$. Error margins are estimated as the largest departure of any one-third of the full times series of $\alpha_{ij}$ and $\eta_{ij}$. The shear of the background flow is normalized with the speed of sound, i.e.,

$$S = sc_{\mathrm{ac}}k_1 = \frac{2\pi s u_{\mathrm{rms}}}{\mathrm{Ma}L}, \tag{36}$$

where $\mathrm{Ma} = u_{\mathrm{rms}}/c_{\mathrm{ac}}$ is the Mach number. In the simulations we work with $s = 0.2$ and $\mathrm{Ma} = 0.05$. One finds

$$\frac{\alpha_{yy}}{\alpha_0} \simeq -\frac{\ell_{\mathrm{corr}}^2}{L^2}. \tag{37}$$

Following Eqs. (12), both streamwise and spanwise $\alpha$ tensor components, $\alpha_{yy}$ and $\alpha_{xx}$, should be negative. When the simulations are done for $\mathrm{Pm} = 1$, $|\alpha_{yy}|$ should strongly exceed the value of $|\alpha_{xx}|$, but this is *not* expected for $\mathrm{Pm} < 1$. Here, the results of two simulations are presented. The first one, for $\mathrm{Pm} = 1$ with $64^3$ mesh points, has $\mathrm{Rm} = 0.2$ and $\mathrm{Re}\cdot\mathrm{Rm} = 0.04$, while the second one, for $\mathrm{Pm} = 0.1$ with $128^3$ mesh points, has $\mathrm{Rm} = 0.25$ and $\mathrm{Re}\cdot\mathrm{Rm} = 0.625$. It is thus possible to find out whether the simulated $\alpha$ effect runs with Rm (which is almost the same) or with $\mathrm{Rm}\cdot\mathrm{Re}$ (which differs by a factor of 10) in both simulations. In both cases $k_f/k_1 = 5$ so that 10 cells can exist in the vertical direction, and therefore, $\ell_{\mathrm{corr}}^2/L^2 \simeq 0.01$.

As predicted, Fig. 3(a) for $\mathrm{Pm} = 1$ shows $\alpha_{yy}$ to be dominant and both diagonal components of $\alpha$ to be basically negative. The amplitude of $\alpha_{yy}/\alpha_0$ is about 0.01, in accordance with Eq. (37) which also leads to $|\alpha_{yy}|/\alpha_0 \simeq 0.01$.

For $\mathrm{Pm} = 1$, $I_2$ is strongly reduced relative to $I_1$ so that the low amplitude of $\alpha_{xx}$ in Fig. 3(a) becomes understandable. For smaller magnetic Prandtl numbers, this reduction does not exist and both $\alpha$ components are of similar amplitude. Close to the upper endplate the intensity stratification changes its sign (due to the boundary conditions) and also a change in the sign of the $\alpha$ effect can be observed there [see Fig. 4(a)]. Without this exception the simulations also confirm that the signs depend only on the sign of the product $g_z S$, as formulated in relations (12).

Moreover, again as predicted, the amplitudes of the diagonal elements of the $\alpha$ tensor increase for decreasing magnetic Prandtl number. In the middle of the channel, the amplitudes of the $\alpha$ components differ by a factor of 10, which exceeds the ratio 1.25 of the two Rm by almost an order of magnitude.

Next, the off-diagonal components of $\alpha_{ij}$ are considered; see Figs. 3(b) and 4(b). As expected, we have $\alpha_{yx} \approx -\alpha_{xy}$, which corresponds to a turbulent pumping velocity in the $z$ direction. This velocity is negative for $k_1 z < 2.5$, corresponding to downward transport, i.e., down the gradient of the turbulent intensity, as expected [1]. Near the top of the domain, the gradient of the turbulent intensity is reversed and

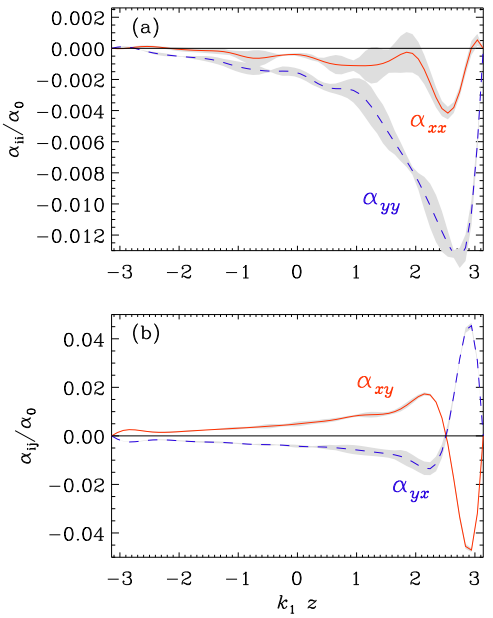


FIG. 3. (Color online) Simulations with positive shear ($s = 0.2$): numerical values for the diagonal elements of the $\alpha$ tensor (top) and the off-diagonal elements (bottom). Error margins are indicated by (gray) shading. Pm = 1, Re = 0.2, Rm = 0.2.

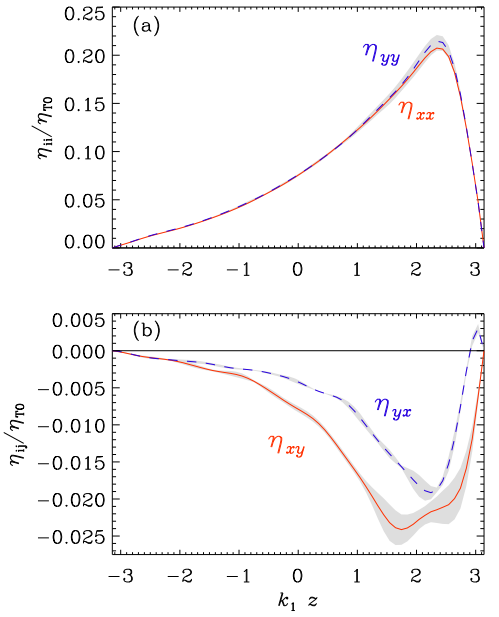


FIG. 5. (Color online) Simulations with $s = 0.2$ for the shear-induced elements of the $\eta$ tensor. Top: Horizontal eddy diffusivities. Bottom: The two shear-current terms, $\eta_{xy}$ and $\eta_{yx}$. Error margins are indicated by (gray) shading. Pm = 1, Re = 0.2, Rm = 0.2.

so is the sign of the pumping velocity $\alpha_{yx}$. The simulations with Pm = 0.1 and 1 lead to the result $\alpha_{yx}/\alpha_0 \simeq -\mathrm{Rm}/10$ [Figs. 3(b) and 4(b)].

## IV. THE DIFFUSIVITY TENSOR

The numerical test-field procedure also allows the simultaneous calculation of the components of the $\eta$ tensor for the same simulation with its vertical stratification of the turbulence intensity. This knowledge is important for the discussion of the question whether turbulence in shear flows can be used for dynamo self-excitation of large-scale magnetic fields. Despite the completely different roles played by the spanwise and streamwise directions, we find the two relevant diagonal components of the diffusivity tensor to be nearly equal; i.e., $\eta_{xx} \approx \eta_{yy}$ [Figs. 5(a) and 6(a)]. This strikingly high degree of isotropy of the turbulent diffusivity

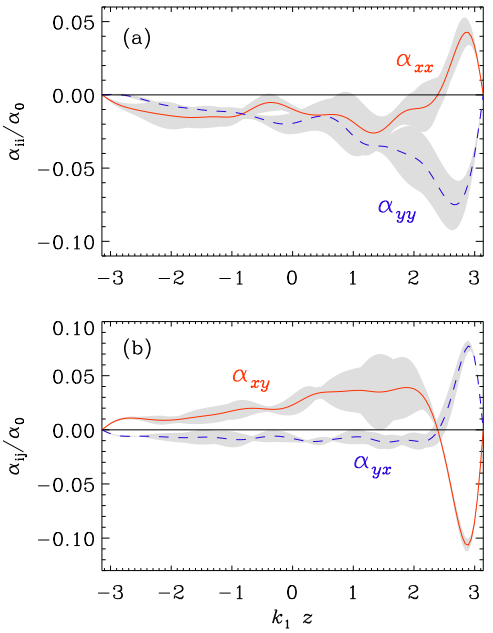


FIG. 4. (Color online) The same as Fig. 3, but for Pm = 0.1, Re = 2.5, Rm = 0.25.

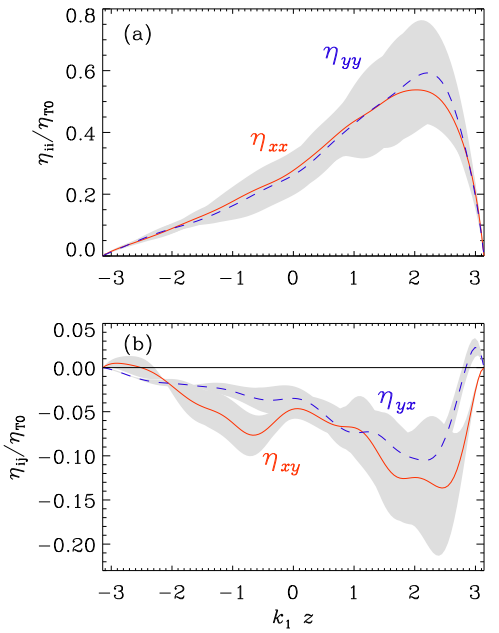


FIG. 6. (Color online) The same as Fig. 5, but for Pm = 0.1, Re = 2.5, Rm = 0.25.

in the $xy$ plane has been noted in earlier simulations of the diffusivity in unstratified turbulent shear flows [2,8,14]. The maximum of $\eta_T = (\eta_{xx} + \eta_{yy})/2$ is about 20% of the reference value $\eta_0$, which agrees with the fact that for $\mathrm{Rm} \ll 1$, $\eta_T/\eta_0 \simeq \mathrm{Rm}$ [16]. For larger Rm (or for smaller Pm) one finds slightly larger numerical values for the eddy diffusivity [Fig. 6(a)].

The data in Figs. 3(a) to 6(a) for $\mathrm{Pm} = 0.1$ and 1 lead to a value of about unity for the normalized $\alpha$ effect, $C_\alpha = \alpha\, L/\eta_T$, which is also typical for rapidly rotating convection [17]. A comparison with the slab-dynamo calculation in [8] leads to $C_\alpha \simeq 10$, as required for self-excitation of the magnetic fields. This condition is not fulfilled for the present simulations.

For the off-diagonal components of the $\eta$ tensor for nonstratified shear flows one finds

$$\eta_{xy} = \eta_x S, \quad \eta_{yx} = \eta_y S, \tag{38}$$

i.e., both are linear in $S$. The calculation of a simple slab dynamo model shows self-excitation for sufficiently large positive $\eta_y$. From quasilinear theory we know, however, that $\eta_y$ is negative definite [8]. For positive shear, the coefficient $\eta_{yx}$ is therefore expected to be negative. This result has also been confirmed for $\mathrm{Rm} \leqslant 200$ for unstratified turbulence [14].

The same sign and the same linear dependence of $\eta_{yx}$ on $S$ also hold for $\eta_{xy}$, but only for Pm of order unity and in the low-conductivity limit. Both conditions are fulfilled for the present simulations. Experiments for liquid metals, however, concern much smaller magnetic Prandtl numbers, for which $\eta_{xy}$ is expected to be positive.

Our numerical simulations for stratified turbulence and with positive shear and $\mathrm{Pm} \leqslant 1$ also produce negative values for both $\eta_{xy}$ and $\eta_{yx}$ [Figs. 5(b) and 6(b)]. The possibility of dynamo action in such nonhelical shear flows [14,18,19] therefore cannot be explained by the so-called shear-current effect.

It is also shown that the vertical stratification of the turbulence intensity does not basically modify the known findings about the eddy diffusivity tensor. Only experiments can finally provide the sign of $\eta_x$, as simulations for such small Pm are not usually possible.

## V. SHEAR FLOW ELECTRODYNAMICS

Following relations (12), the EMF across the channel is

$$\mathcal{E}_x = \alpha_2 g_z S B_0, \tag{39}$$

so that the potential difference $\delta\Phi$ between the walls with distance $D$ is $\delta\Phi = \alpha_2 g_z S D B_0$, and thus

$$\delta\Phi \simeq -0.5\,\mathrm{Rm}\,\ell_{\mathrm{corr}}^2 g_z U B_0 \simeq -\mathrm{Rm}\,\lambda^2\, L U B_0 \tag{40}$$

with $I_2 \simeq 0.5$ for small Pm (Fig. 1, bottom), with $g_z = 2/L$ as the vertical scale height of the turbulence stratification, and with the ratio $\lambda = \ell_{\mathrm{corr}}/L$. The amplitude of the mean shear flow is $U$. Note that, surprisingly, the width $D$ of the channel does not appear in (40) and even the height $L$ has only a weak influence. Hence,

$$\delta\Phi \simeq 10\,\mathrm{Rm}\,\lambda^2 \left[\frac{L}{10\ \mathrm{cm}}\right]\left[\frac{U}{\mathrm{m/s}}\right]\left[\frac{B_0}{\mathrm{kG}}\right] \tag{41}$$

(in mV), so that with (say) $\lambda \simeq 0.1$ and a channel height of 50 cm, a shear flow of 1 m/s subject to a magnetic field of 1 kG would lead to a potential difference of

$$\delta\Phi \simeq 0.5\ \mathrm{Rm}\ [\mathrm{mV}]. \tag{42}$$

For the (maximal) value of $\mathrm{Rm} \simeq 1$ ($u_{\mathrm{rms}} \simeq 1$m/s and $\ell_{\mathrm{corr}} \simeq 5$ cm) the channel should thus provide a potential difference of 0.5 mV between the side walls by the action of the $\alpha$ effect along a spanwise magnetic field. These numbers are quite similar to those of the Riga experiment [1,5]. The basic difference is that in our shear flow the helicity is not prescribed but it is self-consistently produced by the interaction of the stratified turbulence with the background shear.

## VI. CONCLUSIONS

Laboratory studies of homogeneous dynamos are still in their infancy. The only working dynamo where the flow pattern is not strongly constrained by pipes or container walls is the experiment in Cadarache [20], where, however, the effects of soft iron play an important and not well understood role [21]. The present proposal of measuring the $\alpha$ effect in an *unconstrained* turbulent flow would therefore be a major step forward. In such an experiment, the pseudoscalar necessary for producing helicity comes from the stratification of turbulent intensity giving rise to a polar vector and the vorticity associated with the shear flow giving rise to an axial vector. Thus, the basic effects in the theory of turbulent dynamos, which are usually considered as special properties of *rotating* and stratified fluids, can also be found for the plane-shear flows, i.e., without global rotation.

The present work yields a detailed prediction of the sign and magnitude of the components of both $\alpha$ and $\eta$ tensors. It may motivate the construction of a suitable experiment using liquid metals to achieve a measurable $\alpha$ effect. The necessary vertical stratification of turbulence intensity must be experimentally imitated using grids with nonuniform mesh sizes and/or walls of increasing/decreasing roughness in the vertical direction.

We have shown that in stratified turbulence driven in a plane shear flow, a measurable $\alpha$ effect should exist. Here, the key problem is the smallness of the magnetic Prandtl number. For $\mathrm{Pm} \leqslant 1$, the quasilinear theory and the possible nonlinear numerical simulations lead to very similar results. With the quasilinear theory we have shown that, even for fluids with very small magnetic Prandtl numbers, stratified shear flow turbulence leads to an $\alpha$ effect that can be realized in an experiment with liquid metals such as sodium ($\mathrm{Pm} \simeq 10^{-5}$) and gallium ($\mathrm{Pm} \simeq 10^{-6}$). Such small magnetic Prandtl numbers cannot be simulated with present-day numerical codes.

In fact, it may not be possible that such flows could produce a supercritical dynamo in the conceivable future. Nevertheless, even in the subcritical case, an $\alpha$ effect should be measurable, which would thus open the possibility of detailed comparisons

among theory, simulations, and experiments. Once such comparison is possible, there will be more details that should be investigated. One of them concerns the modifications of the results in the presence of imperfect scale separation in space and time. For oscillatory dynamos, this effect can significantly lower the excitation conditions for the dynamo compared to standard mean-field estimates [22].

**ACKNOWLEDGMENTS**

Financial support from the European Research Council under AstroDyn Research Project 227952, the Swedish Research Council under Grant Nos. 621-2011-5076 and 2012-5797, and the Research Council of Norway under FRINATEK Grant No. 231444 is gratefully acknowledged.

[1] F. Krause and K.-H. Rädler, *Mean-Field Magnetohydrodynamics and Dynamo Theory* (Pergamon Press, Oxford, UK, 1980).
[2] A. Brandenburg, Astron. Nachr. **326**, 787 (2005).
[3] G. Rüdiger and R. Hollerbach, *The Magnetic Universe: Geophysical and Astrophysical Dynamo Theory* (Wiley-VCH, Berlin, 2004).
[4] V. Noskov, S. Denisov, R. Stepanov, and P. Frick, Phys. Rev. E **85**, 016303 (2012).
[5] M. Steenbeck, I. M. Kirko, A. Gailitis, A. P. Klawina, F. Krause, I. J. Laumanis, and O. A. Lielausis, Monats. Dt. Akad. Wiss. Berlin **9**, 714 (1967).
[6] R. Stepanov, R. Volk, S. Denisov, P. Frick, V. Noskov, and J.-F. Pinton, Phys. Rev. E **73**, 046310 (2006).
[7] P. Frick, S. Denisov, V. Noskov, and R. Stepanov, Astron. Nachr. **329**, 706 (2009).
[8] G. Rüdiger and L. L. Kitchatinov, Astron. Nachr. **327**, 298 (2006).
[9] M. Schrinner, K.-H. Rädler, D. Schmitt, M. Rheinhardt, and U. R. Christensen, Geophys. Astrophys. Fluid Dynam. **101**, 81 (2007).
[10] K.-H. Rädler and R. Stepanov, Phys. Rev. E **73**, 056311 (2006).
[11] G. Rüdiger, Astron. Nachr. **299**, 217 (1978).
[12] L. L. Kichatinov, Astron. Astrophys. **243**, 483 (1991).
[13] N. E. L. Haugen, A. Brandenburg, and W. Dobler, Phys. Rev. E **70**, 016308 (2004).
[14] A. Brandenburg, K.-H. Rädler, M. Rheinhardt, and P. J. Käpylä, Astrophys. J. **676**, 740 (2008).
[15] http://pencil-code.googlecode.com
[16] S. Sur, A. Brandenburg, and K. Subramanian, Month. Not. R. Astron. Soc. **385**, L15 (2008).
[17] P. Käpylä, M. Korpi, and A. Brandenburg, Astron. Astrophys. **500**, 633 (2009).
[18] T. A. Yousef, T. Heinemann, A. A. Schekochihin, N. Kleeorin, I. Rogachevskii, A. B. Iskakov, S. C. Cowley, and J. C. McWilliams, Phys. Rev. Lett. **100**, 184501 (2008).
[19] I. Rogachevskii and N. Kleeorin, Phys. Rev. E **68**, 036301 (2003).
[20] R. Monchaux, M. Berhanu, M. Bourgoin, M. Moulin, Ph. Odier, J.-F. Pinton *et al.*, Phys. Rev. Lett. **98**, 044502 (2007).
[21] A. Giesecke, C. Nore, F. Stefani, G. Gerbeth *et al.*, New J. Phys. **14**, 053005 (2012).
[22] M. Rheinhardt and A. Brandenburg, Astron. Nachr. **333**, 71 (2012).